PERGAMON

International Journal of Heat and Mass Transfer 41 (1998) 2781–2798

International Journal of HEAT and MASS TRANSFER

Thermal interface resistance and subsurface effusivity of submicron metallic films on dielectric substrates: an experimental method for simultaneous determination

N. Hmina[a], Y. Scudeller[b]*

[a]*Laboratoire de mécanique des fluides et transfert thermique, Kénitra, Maroc*
[b]*Equipe de Thermique des Interfaces et de Microthermique, Laboratoire de Thermocinétique, URA CNRS 869, ISITEM, Nantes, France*

Received 5 January 1996; in final form 7 October 1997

Abstract

Adhesion and homogeneity of thin films are closely related to the physical and chemical subsurface properties. Thermal interface resistance characterizes the transition region and inhomogeneities.

An original method of simultaneous measurement of the thermal interface resistance submicronic film-substrate and effusivity of the substrate is presented. The measurement consists of analyzing the cooling phase which follows the temperature increase of the film by means of a short laser pulse (20 ns). The temperature is deduced from the electrical resistance of the film. The methodology uses a large analog bandwidth and a signal processing. In this way, the interface resistance as small as 10^{-8} m^2 K W^{-1} may be detected if the analysis is performed before the two microseconds. The effusivity characterizes a depth of a few μm into the substrate.

The principle of the method and experimental arrangement are described. A theoretical model and a sensitivity analysis are presented. The experiments are on a copper–glass and copper–alumina microstructures. The effects of physical and chemical treatments are quantified. Measurements on thermal interface resistance are in the order of magnitude of 10^7 m^2 K W^{-1} with an uncertainty of about 30%.

Nomenclature

a_1 diffusivity of the film [m^2 s^{-1}]
a_2 diffusivity of the substrate [m^2 s^{-1}]
A_0 heated surface [m^2]
A_1 section of the film [m^2]
A_{1c} section of the connection bars [m^2]
A_2 section of the substrate [m^2]
b_1 effusivity of the film [J m^{-2} K^{-1} s$^{-1/2}$]
b_2 effusivity of the substrate [J m^{-2} K^{-1} s$^{-1/2}$]
b^* film effusivity on the substrate one
$c_1\rho_1$ heat capacity of the film per unit volume [J m^{-3} K^{-1}]
$c_2\rho_2$ heat capacity of the substrate per unit volume
D radial dimension of the irradiation
$\tilde{f}$ Fourier transform
Fo_1 Fourier number of the film
I electrical current [A]
n, m integer
p complex variable
P_0 total power of laser beam [W]
q_0 pulse energy [J]
Q_0 energy density of pulse [J m^{-2}]
Q flux per unit volume [W m^{-3}]
r_0 mean radius of beam [m]
R_c thermal interface resistance [m^2 K W^{-1}]
R^* undimensionless resistance
t time [s]
t_0 reference time [s]
t_p pulse duration [s]
t^* pulse duration on diffusion time of the film
T temperature [K]
T_1 temperature of the film [K]
T_2 temperature of the substrate [K]
T_i initial temperature of the film [K]
S_b undimensionless sensitivity to substrate effusivity

* Corresponding author. Fax: 00-33-02-40-68-31-41; e-mail scudelle@isitem.uni-nantes.fr.

0017-9310/98 $19.00
PII: S0017-9310(98)00363-3

S_c undimensionless sensitivity to capacity
S_R undimensionless sensitivity to interface resistance
S_t reduced sensitivity to time
S_η sensitivity coefficient of $\theta(t)/\theta_0$ to parameter η
S_η^0 sensitivity coefficient of $\theta(t)/\theta_{max}$ to parameter η
x_1 film thickness [m]
x_2 substrate thickness [m]
y_0, z_0 lateral dimensions of the heated surface [m]
y_1, z_1 lateral dimensions of the film [m]
y_2, z_2 lateral dimensions of the substrate [m].

Greek symbols
δ penetration depth [m]
δV electrical potential variation [V]
δV_i initial electrical potential [V]
θ_0 reference temperature rise of the film [K]
θ_1 temperature rise of the film [K]
θ_2 temperature rise of the substrate [K]
θ_{max} maximal rise in the film temperature [K]
θ_2^* mean temperature of the substrate
θ_c^* reduced temperature in the interface film-substrate
θ_s^* reduced temperature of the film surface
θ_{moy}^* mean temperature of the film
κ_λ extinction coefficient [m^{-1}]
λ_1 conductivity of the film [W m^{-1} K^{-1}]
λ_2 conductivity of the substrate [W m^{-1} K^{-1}]
ρ_λ directional monochromatic reflectivity of the film
σ electrical conductivity [Ω^{-1} m^{-1}]
σ^* roughness random [m]
σ_b uncertainty on effusivity of the substrate
σ_C uncertainty on coating thermal capacity
σ_R uncertainty on R_c
σ_t uncertainty on time
σ_θ uncertainty on temperature measurement
τ time constant [s]
ϕ heat flux density [W m^{-2}]
φ_a heat flux in axial direction [W]
φ_r heat flux in radial direction [W].

1. Introduction

The characterization of the thermophysical properties of the microsystems such as Fast Electronic Devices, Optical Microcomponents is an important field for material sciences in understanding the mechanisms of degradation [1, 2]. Elaboration of submicronic solid films leads to a structural problem which involves thermophysical properties of the substrates. Homogeneity and adhesion are a combination of deposition mechanisms with physical and chemical properties of the substrate. The transition region (b) (Fig. 1) in a scale of a few nanometers corresponds to the variations of physical properties of the structure from the film to the substrate which occurs impurities and contaminants. Atomic interdiffusion and surface profile play an essential role in the localization of the transition region. Two other regions (a) and (c) corresponding to the structural defects may be defined. In heat transfer point of view, (a), (b), (c) constitute the interfacial region. A temperature drop states when heat flows from the film to the substrate.

The temperature field is perturbed inside a zone larger than the transition region—due to spreading of the heat flux—but remains generally thin compared to medium thickness [3, 4]. The thermal resistance between the two isothermal surfaces T_1 and T_2 outside the perturbed zone is given by:

$$R = \frac{T_1 - T_2}{\phi} \tag{1a}$$

ϕ denotes the heat flux density.

The thermal interface resistance model introduces a discontinuity of temperature by extrapolating the temperature distributions outside the perturbed region. The two temperatures T_1^0 and T_2^0, obtained by the extrapolation define a theoretical interface. Then, the thermal interface resistance may be introduced on writing:

$$R_c = \frac{T_1^0 - T_2^0}{\phi}. \tag{1b}$$

In (1a) and (1b), R_c appears as a perturbation representing the amount of thermal resistance due to the presence of structural defects and contaminants:

$$R_c = R - R_0. \tag{1c}$$

R_0 is the thermal resistance of the transition region with a perfectly abrupt interface under assumptions that properties are equivalent to bulk materials.

This simple model may be invalid in very fast transient regime as soon as time of heat diffusion into the disturbed region is not negligible compared to structure one. Heat diffusion must be taken into account. In practice, if thickness of the disturbed region does not exceed a few nanometers (case of metal on glass) temperature distribution of this region is established, and the behavior may be characterized by relation (1c). The thermal interface resistance is able to quantify the rates of defects due to the process. R_c is approximately placed between 10^{-8} m^2 K W^{-1} and 10^{-6} m^2 K W^{-1} for thin film-substrate structures [5–11].

This article presents a method of simultaneous experimental determination of thermal interface resistance of a submicronic film and effusivity of the subsurface of a substrate. The principle and an experimental arrangement are described in detail. A heat diffusion model is proposed for experimental identification. A sensitivity study gets the role of the various parameters and determines a basic approach for experimental analysis. Moreover, incertitudes of the measurement are given vs. the structures and experimental parameters. This study carries on the limits of the detection which appear very dependent on the substrate. Experimental results on pul-

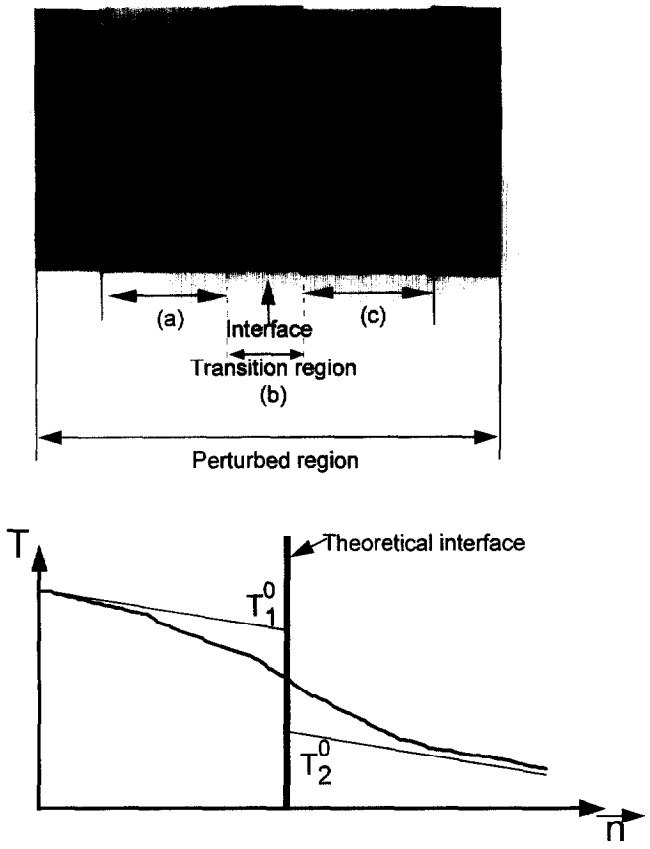

Fig. 1. Thermal contact resistance.

verized submicronic copper film on glass and alumina are presented and the role of the contamination is studied.

2. Principle of the method

The method is illustrated in Fig. 2. The metallic thin film, initially at a temperature T_i, is irradiated by a laser pulse of 20 nanoseconds duration with a high energy less than 0.5 J cm^{-2}. After a peak of temperature, T_{max}, the transient temperature decrease of the film (cooling phase) is analyzed. The thermophysical properties of the structure may be identified. Simultaneous measurement of thermal interface resistance and effusivity of the substrate may be performed by fitting the early times of this profile; in practice, during a few hundreds of nanoseconds. Observations are so short that temperature gradients are confined within a few micrometers depth.

As a matter of fact, the penetration depth δ is approximately given by the relation:

$$\delta = 4\sqrt{a_2 t}$$

in which a_2 is the thermal diffusivity of the substrate.

Thus, the experiment provides a parameter at micron scale, named subsurface effusivity for this reason:

$$b_2 = \sqrt{\lambda_2 c_2 \rho_2}$$

λ_2 and $c_2\rho_2$ are the thermal conductivity and the specific heat of the substrate.

First, the identification of the parameters (R_c, b_2) is performed on a normalized thermogram by a temperature rise $\theta_0 = (T_0 - T_i)$, located near the peak one θ_{max} to ensure an analysis independent of the pulse energy q_0. θ_{max} is not generally used for normalization because its measurement is inaccurate. The location of θ_0 depends on one hand, on detection capability, in terms of time response and electromagnetic perturbations, of temperature, and on the other hand, on the sensitivity of the fraction $\theta(t)/\theta_0$ to the estimated parameters.

Secondly, the radial dimension D of the irradiation has to be considerably higher than the penetration depth. This configuration ensures one-dimensional heat transfer and consequently is sensitive to the interface (heat flux lines are normal to the interface).

The temperature measurement is deduced from the electrical resistivity variation of the metallic film. A con-

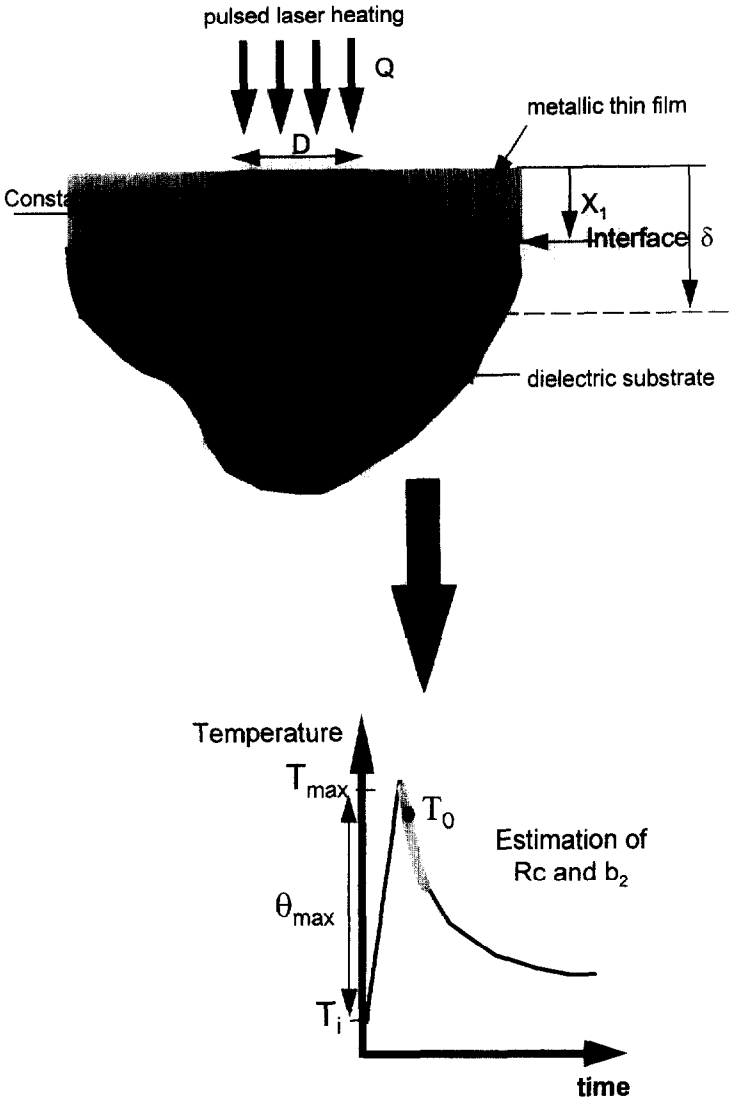

Fig. 2. Principle of the measurement.

stant current I is supplied and electrical potential difference δV is measured along the film (Fig. 2(b)). δV is related to the temperature T of the film by the following expression:

$$\delta V = \frac{F(T)*I}{\sigma(T)} \tag{2}$$

σ is the electrical conductivity of the film and F, a function which characterizes geometry of the heated region. The thermomechanical strains do that F is also a function of temperature [12]. For pure metals, variation of σ with T is higher. Calibration shows the linearity of $(\delta V - \delta V_i)$ with $(T - T_i)$ in a small range of temperature:

$$\Delta V = \delta V - \delta V_i = K(T - T_i). \tag{3}$$

It may be shown that K increases with electrical resistance of the film and the current. Response can be sufficiently high (few mV K^{-1}) to analyze a single thermogram and consequently avoid a repetition rate which induced some bias due to the energy drift. Relation (3) shows that the ratio of two difference of potential is equal to the temperature differences one and therefore, determination of K is not necessary.

In this way, during the two microseconds, interface resistance (as small as 10^{-8} m^2 K W^{-1}) and simultaneously the subsurface effusivity can be detected. Sensitivity of the method depends on the film thickness, the material used for the substrate and the accuracy of temperature measurement.

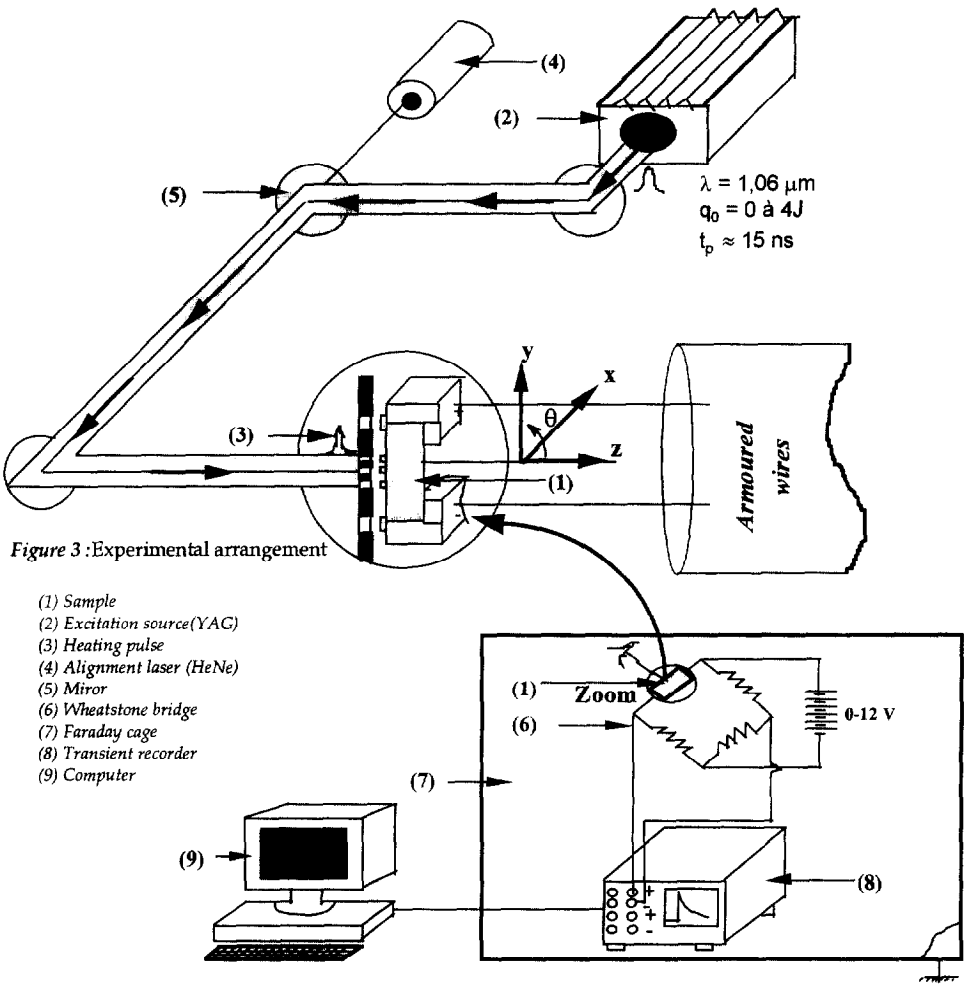

Figure 3 :Experimental arrangement

(1) Sample
(2) Excitation source(YAG)
(3) Heating pulse
(4) Alignment laser (HeNe)
(5) Miror
(6) Wheatstone bridge
(7) Faraday cage
(8) Transient recorder
(9) Computer

Fig. 3. Experimental arrangement.

3. Experimental arrangement

The experimental arrangement (Fig. 3) is composed of a YAG : Nd laser, the sample (1), integrated in a resistive bridge (6), an acquisition and data processing system (8).

The laser (λ = 1.06 μm) supply high energy pulses (0–4 J) of about 20 ns. Optical elements ensure the uniformity of intensity under a spot of 10 mm of diameter. A HeNe laser (4) allows the alignment of the target with the incident beam. The sample is held on a micro-stage $xyz\theta$ and cooled by a circulation of fluid.

The sample is the metallic film deposited on a bulk substrate of a few millimeter thickness (section of about 25×75 mm^2) and connected with two copper blocks (Fig. 4(a)). The heated region is about 10 mm diameter. The film is a strip of 500 μm wide (Fig. 4(b)). The two ends enlarge progressively to get in contact with the blocks. A copper film of a few hundreds of nm supplied by a current of 50 mA gives a sensitivity of about 1–2 mV K^{-1}. The

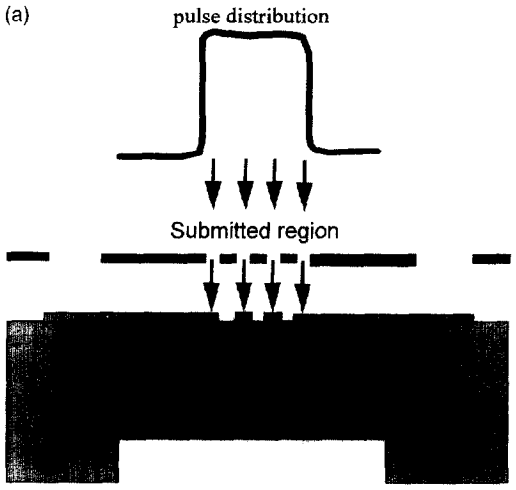

Fig. 4(a). Sample and its diaphragm.

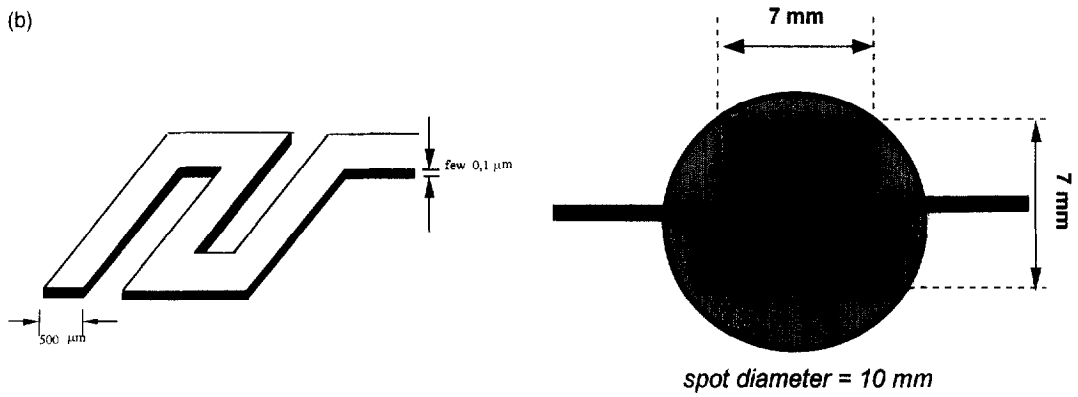

Fig. 4(b). The heated region zoom.

shape of the film is achieved by means of a deposition mask which is held on the upper side of the substrate. This arrangement is preserved during laser shots so that the mask will have a role of an optical diaphragm.

The resistive bridge is supplied by a 0–12 V source. A resistance limits the current. Equilibrium of the bridge removes the initial value (tension δV_i) corresponding to the temperature T_i of the film.

The transient recorder (8) which operated with a sampling of 50 MHz and an analog bandwidth of 25 MHz. Data are processed on a computer. The sample and its resistive bridge, the transient recorder are inside a Faraday cage to reduce electromagnetic perturbations.

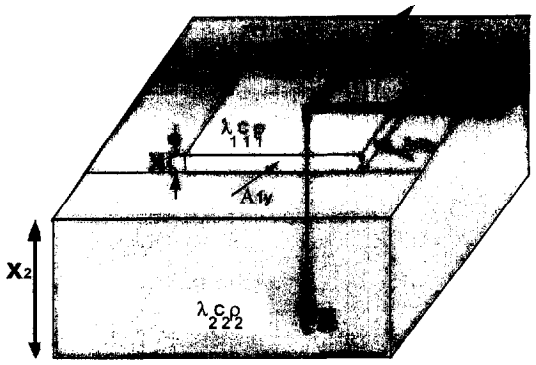

Fig. 5. Geometry of the general model.

4. Heat diffusion model

The experiment is supported by a theoretical model, especially for the identification of the parameters. The heat diffusion model gives the temperature rise of the metallic thin film, in imperfect contact with a substrate, heated by a laser pulse. The studied structure is on Fig. 5. It is composed of the thin film (section A_1, dimensions y_1, z_1 and x_1 thick) on its substrate (section A_2, lateral dimensions y_2, z_2). The thermophysical properties of the materials are assumed homogeneous and independent of temperature. The heated area is equal to A_1. The substrate is a semi-finite body because x_2 is higher than the heat penetration depth δ. Convection and radiation are negligible. Imperfect contact is taken into account by means of a thermal interface resistance R_c uniform and independent of time. One dimensional approach is used for identification. Effects of semi-transparency and pulse length are analyzed. In addition, a multidimensional model (Appendix) quantify effects of the film shape and the dimension of the laser spot. The analysis brings a validity criteria of the 1-D model.

4.1. One-directional approach

Capacitive model. The thermal conductivity of the film is assumed infinite. The initial temperature is the adiabatic one. The lumped system is given by:

(1)

$$c_1\rho_1 x_1 \frac{\mathrm{d}\theta_1}{\mathrm{d}t} = \frac{\theta_2 - \theta_1}{R_c} \forall t > 0 \quad \text{in } x = 0 \tag{4.1.1}$$

$$\text{at } t = 0 \quad \theta_1(0) = \theta_{\max} \quad \text{with } \theta_{\max} = \frac{Q_0}{c_1\rho_1 x_1} \tag{4.1.2}$$

(2)

$$\frac{1}{a_2}\frac{\partial\theta_2(x,t)}{\partial t} - \frac{\partial^2\theta_2(x,t)}{\partial^2 x} = 0 \quad \forall x > 0, t > 0 \tag{4.2.1}$$

$$-\lambda_2 \frac{\partial \theta_2}{\partial x} = \varphi(t) \tag{4.2.2}$$

$$x \to \infty \quad \theta_2 \to 0 \tag{4.2.3}$$

$$\text{at} \quad t = 0 \quad \theta_2(x,0) = 0 \quad \forall x > 0. \tag{4.2.4}$$

The temperature rise of the film is:

$$\theta_1(t) = \frac{\theta_{\max}}{2\beta}\left\{(3+\beta)\exp\left[\frac{\alpha t}{4\tau}(1+\beta)^2\right]\right.$$
$$\times \operatorname{erfc}\left[-\sqrt{\frac{\alpha t}{4\tau}}(1+\beta)\right] - (3-\beta)$$
$$\left.\times \exp\left[\frac{\alpha t}{4\tau}(1-\beta)^2\right]\operatorname{erfc}\left[-\sqrt{\frac{\alpha t}{4\tau}}(1-\beta)\right]\right\} \tag{5}$$

$\operatorname{erfc}(u)$ is the complementary of the error function

$$\operatorname{erfc}(u) = \frac{2}{\sqrt{\pi}}\int_u^{\infty} e^{-v^2}\,dv$$

and parameters τ, α, β have the following expressions:

$$\tau = c_1\rho_1 x_1 R_c \quad \alpha = \frac{x_1}{\lambda_2 R_c}\frac{c_1\rho_1}{c_2\rho_2} \quad \beta = \sqrt{1-\frac{4}{\alpha}}.$$

The sensitivity of R_c to the surface temperature is the most important one at the time defined by τ. It may be observed that τ is independent of the thermophysical properties of the substrate [13]. τ is low when R_c is situated between 10^{-8} and 10^{-7} m^2 K W^{-1}.

The temporal profile depends on a dimensionless parameter α which is linked to the thermophysical properties of materials in contact.

Dimensionless temperature profile $\theta_1/\theta_{\max}$ (Fig. 6) tends to an exponential law ($\alpha = 0$) for small values of α. Raising of R_c involves mainly an expansion of time scale.

The detectability of R_c (10^{-8}–10^{-6} m^2 K W^{-1}) for 200 nm and 1 μm copper films on glass and alumina substrates is of a microsecond scale (Fig. 7). Low variations of interface resistance may be detected easily as effusivity of the substrate is high. Accuracy under alumina substrate ($b_2 = 8900$ J m^{-2} K^{-1} s$^{-1/2}$) is higher than glass substrate ($b_2 = 1500$ J m^{-2} K^{-1} s$^{-1/2}$).

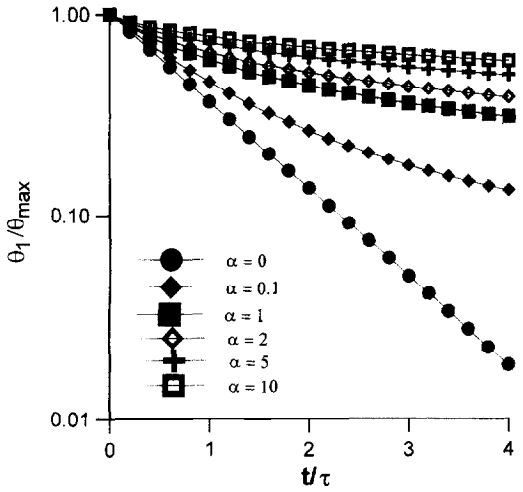

Fig. 6. The reduced cooling $\theta_1/\theta_{\max}$ vs. t/τ and α.

Heat diffusion inside the film. The surface temperature, the temperature at interface, the mean temperature of the film due to a Dirac function for heat source, have been computed. Dimensionless profiles θ_c^*, $\theta_c^*$and θ_{moy}^* in function of the Fourier number $Fo_1 (Fo_1 = a_1 t/(x_1)^2)$; depending on effusivities ratio b^* ($b^* = b_1/b_2$) and on a dimensionless resistance R^* ($R^* = \lambda_1 R_c/x_1$) [14] (Fig. 8) shows for ($R^* = 0$) that temporal profiles meet when Fo_1 became greater than 0.5. This one is larger than effusivities ratio is high. When $b^* > 1$, responses are practically superposed beyond $Fo_1 \approx 5$. It follows that a copper film of 1 μm is isothermal after $t \approx 50$ ns. This duration remains small compared to observation time (few hundredths of nanoseconds) so that heat diffusion inside the film may be neglected.

Pulse duration effect. The pulse duration is not negligible compared to the observation time. The mean temperature response through the film due to a finite pulse (amplitude φ_0 and t_p width) is superposed to the contact temperature due to an infinite pulse at a reduced time ($t^* = a_1 t_p/(x_1)^2$), depending on b^* and R^*. The maximal temperature decreases when t^* increases (Fig. 9). This comes from the progressive decreasing of the heat flux density which is required for the conservation of the pulse energy when t_p increases. On the other hand, the cooling phase spreads of the response to a Dirac pulse, all the more than t^* increases. Temperatures are after progressively superposed quickly that t^* is weak. For the perfect contacts ($R^* = 0$), it is suitable to use very quick pulses for considering them as infinitely short. With 1 μm copper deposited on the glass and submitted by a pulse of 20 ns ($t^* = 2$), it must wait 100 ns ($Fo_1 \approx 10$) so as the models will meet perfectly. The same thresholds are approximately obtained for the imperfect contacts.

Semi-transparency effect. This effect has been studied on an optically thick film. Spatial profile of the laser heating is characterized by the monochromatic absorption coefficient κ_λ. The effects of the dispersion are neglected. $\bar{\theta}_1$ lets appear the Fourier number Fo_1 and the optical layer of the film. The initial amplitude of the mean temperature decreases with $\kappa_\lambda x_1$ (Fig. 10). When $\kappa_\lambda x_1 = 5$, the temperature moves very slightly away from the impulsion response for Fourier numbers $Fo_1 < 1$. Evolutions meet when $Fo_1 > 1$. With a copper film ($\kappa_\lambda \approx 5 \cdot 10^{+7}$ m^{-1}) the layer x_1 for which the semi-transparency effect is not felt, is about 100 nm. When $\kappa_\lambda x_1 \approx 10$, responses are practically superposed. This result is proved for the whole practical values of R^* and b^*.

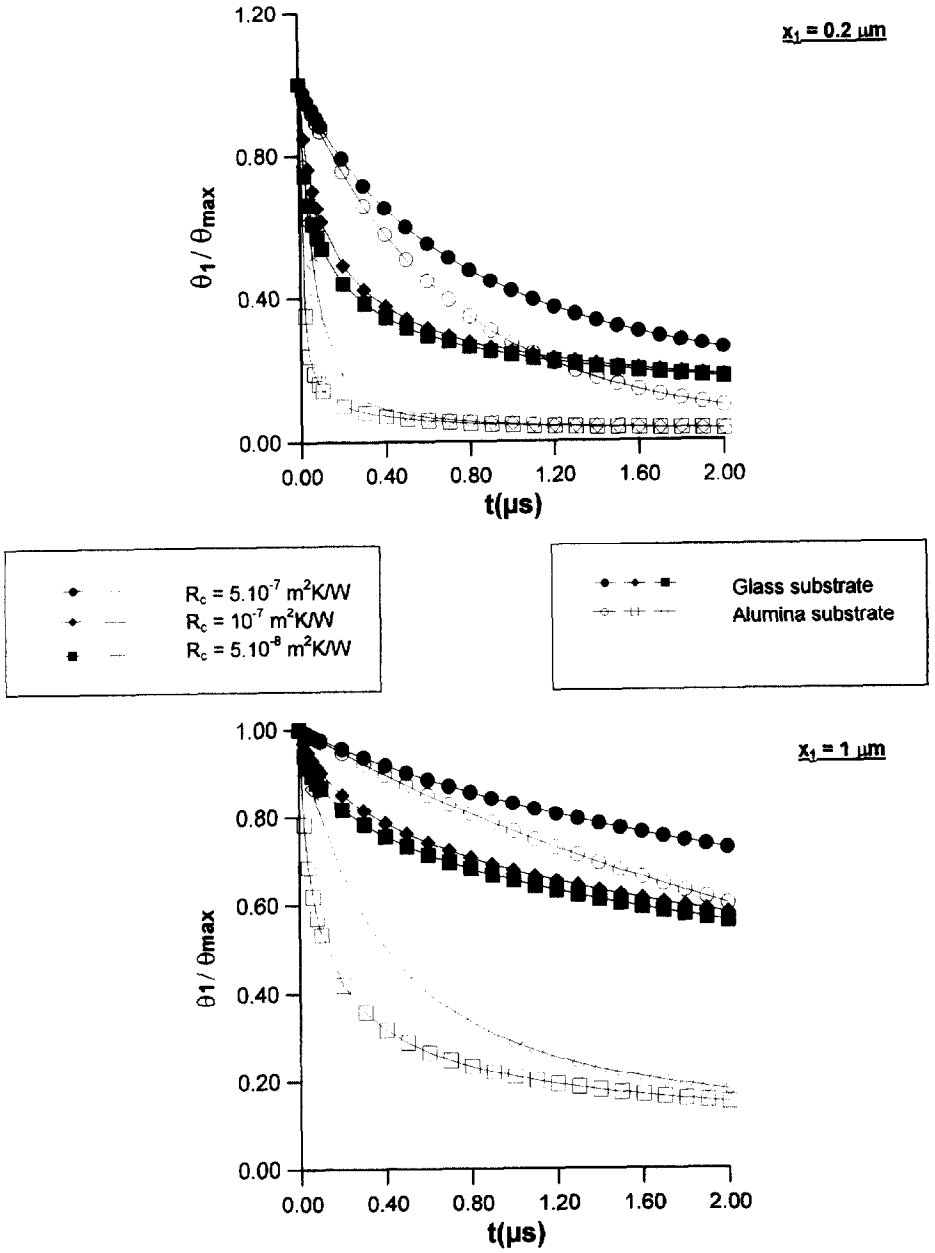

Fig. 7. The reduced cooling copper–glass and copper–alumina structure for different contact resistance R_c. $x_1 = 200$ nm, $x_1 = 1$ μm.

4.2. Bidimensional heat diffusion

The effect of the connection bars has been studied. The film is taken as a rectangular strip of y_1 long and z_1 wide and laser heating is located under $z_0 = z_1$ and $y_0 < y_1$ (Fig. 11). Radial effect has been quantified to compute the axial heat flux φ_a through section A_0 and the radial heat flux φ_r through the section of the connection bars. Mean values have the following expressions:

$$\varphi_a = -\frac{A_0}{y_0}\int_0^{y_0} \lambda_1 \left(\frac{\partial \theta_1}{\partial x}\right)_{x=x_1,y} \mathrm{d}y \tag{6}$$

$$\varphi_r = -\frac{A_{1z}}{x_1}\int_0^{x_1} \lambda_1 \left(\frac{\partial \theta_1}{\partial y}\right)_{x,y=y_0} \mathrm{d}x. \tag{7}$$

One-dimensional heat transfer is considered inside the substrate in order to dissociate the 3-D spreading effect. Shapes corresponding to $y_0/y_1 \approx 0.7$, provide a high ratio

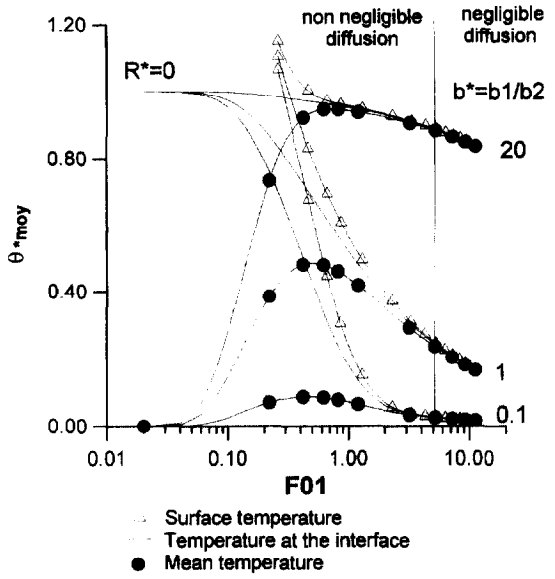

Fig. 8. Comparison of reduced heatings of the coating surface and of the contact coating-substrate with the mean heatings for $R^* = 0$. Influence of b_1/b_2.

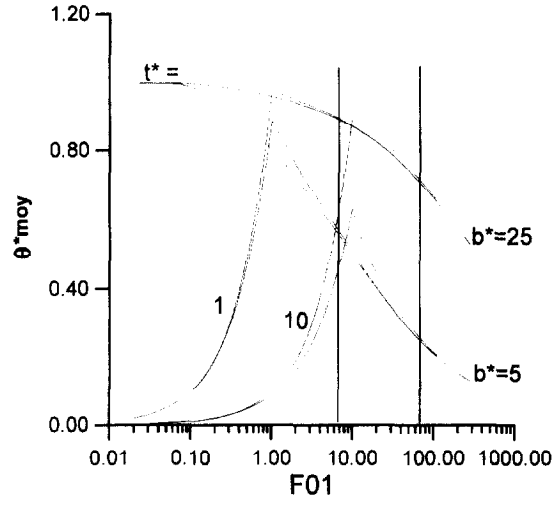

Fig. 9. Comparison of the coating response to rectangular excitations of different duration with the impulsion response.

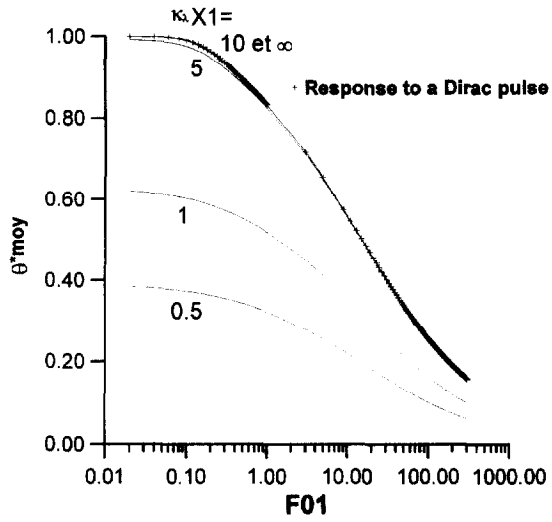

Fig. 10. The semi-transparent effect of the coating on the temperature. Influence of the optical thickness $\kappa\lambda_1 x_1$, $b^* = 5$.

$(\varphi_a/\varphi_r) \approx 10^{-3}$ and do that φ_r is independent of R_c (Fig. 12). This ratio is higher with a ceramic than a glass substrate. Radial heat diffusion may be neglected in the film. It must be taken into account under other shapes. A shape of $y_0/y_1 \approx 10^{-2}$, gives $(\varphi_a/\varphi_r) \approx 20$ (1 μm copper on glass), and it is not completely negligible on temperature profile.

4.3. Three-dimensional heat diffusion

Three-dimensional temperature profiles for a metallic strip ($2z_0$ length and $2y_0$ wide) has been studied (Appendix). It appears that heat diffusion is mainly 1-D in early times and 3-D effects involves later. Observations from 1–2 μs corresponds to a penetration depth δ smaller than

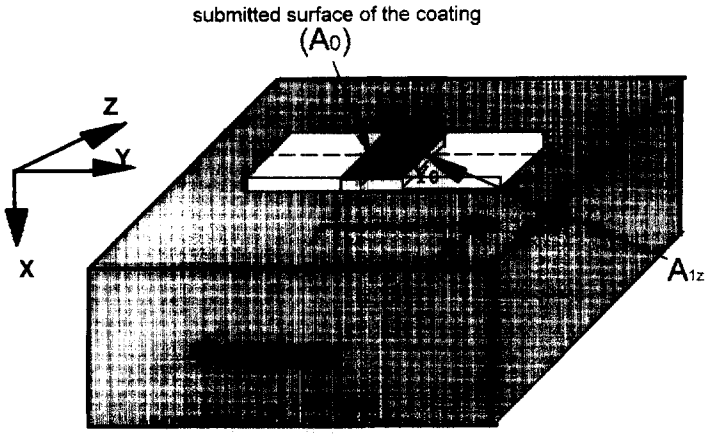

Fig. 11. Bi-dimensional geometry.

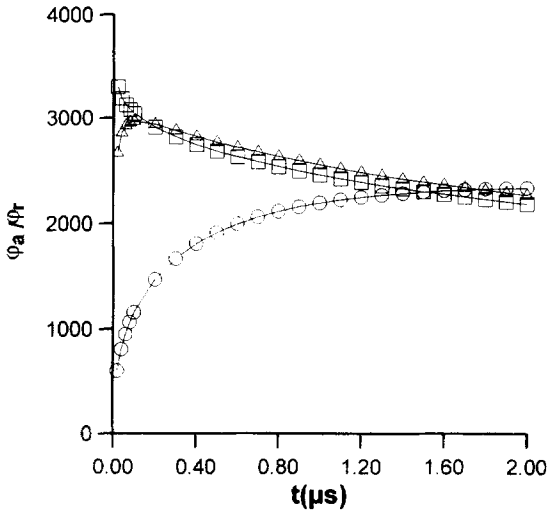

Fig. 12. Comparison of the axial φ_a and radial φ_r flux for 1 μm copper–glass (the used dimensions during the experience).

20 μm and considerably lower than the strip (500 μm). Error on temperature rise is less than 1% for all values of R_c with 200–1000 nm copper films on glass or alumina (Fig. 13).

4.4. Conclusion

Heat diffusion inside submicronic metallic films does not have a significant effect. The temperature gradient is uniform since $a_1 t/(x_1)^2 > 5$. A film of 1 μm is isothermal as soon as $t > 50$ ns. The pulse duration t_p does not have a significant effect if time does not exceed 10 t_p. After a time corresponding to $Fo_1 \approx 50$, parameters can be identified. Ends of the metal strip does not introduce any errors (2-D effects). Three-dimensional effects inside the substrate do not occur before a few μs.

According to this analysis, 1-D capacitive model may be used for parameters estimation. We can see only four parameters θ_{max}, R_c, $C_1 = c_1\rho_1 x_1$, $b_2 = \sqrt{\lambda_2 c_2 \rho_2}$.

5. Sensitivity, precision and detection threshold

Sensitivity coefficients. The sensitivity coefficient of the fraction $\theta^* = \theta(t)/\theta_{max}$ to a parameter η has the following expression:

$$S_\eta^0(t) = \frac{\eta}{\theta_{max}}\left|\frac{\partial\theta(t)}{\partial\eta}\right|$$

$$\eta = R_c, C_1, b_2. \tag{8a}$$

Identification needs the measurement of a fraction $\theta(t)/\theta(t_0)$. The sensitivity coefficient is then given by:

$$S_\eta(t) = \theta^*(t_0)\cdot S_\eta^0(t) - \theta^*(t)\cdot S_\eta^0(t_0). \tag{8b}$$

Temporal variations of S_R have a maximum between $t = 50$ ns and $t = 200$ ns for a copper film of 500 nm (Fig. 14(a) and (b)) in the range of $R_c = 10^{-7}$ m^2 K W^{-1}. Maximum decreases if t_0 increases. The position of the maximum is approximately reminded from t_0. The alumina substrate leads to a high sensitivity on R_c. Precision of measurement will be improved.

Sensitivity coefficients to C_1 and b_2 (Fig. 14(c)–(f)) have also a maxima. Positions increase strongly with b_2. For conducting substrates, such as alumina, S_R and S_c are correlated (Fig. 14(b) and (f)). Consequently, only R_c and b_2 may be identified and an estimation of C_1 has to be done. For insulating substrates, such as glasses, S_c and S_b are correlated (Fig. 14(c) and (e)). R_c and one of the two other parameters can be identified simultaneously.

Precision. Errors on R_c has the following expression:

$$\sigma_R = \sigma'_R + \sigma''_R \tag{9}$$

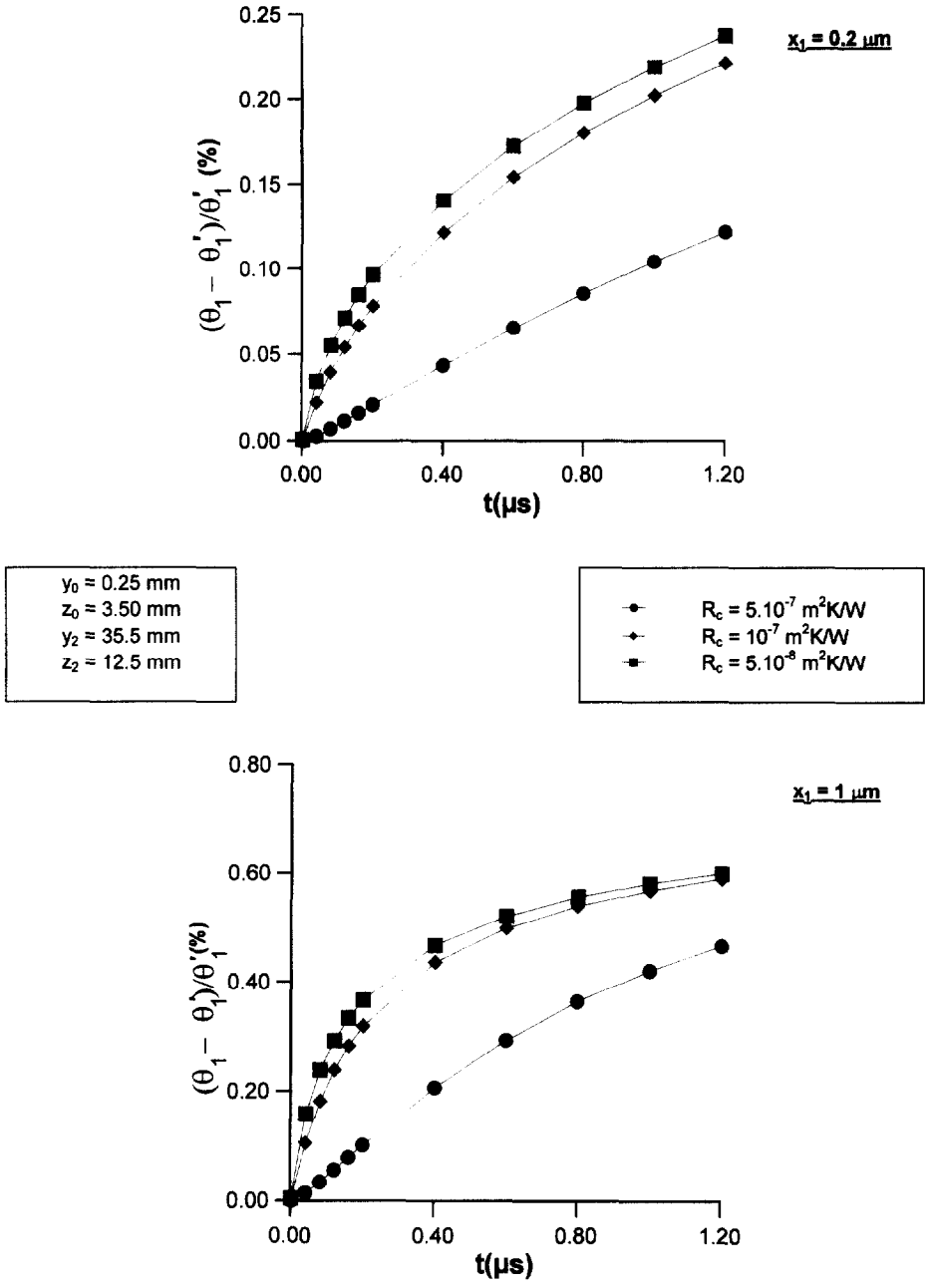

Fig. 13. Comparison of calculated heating by 1-D and 3-D model for a copper–glass structure.

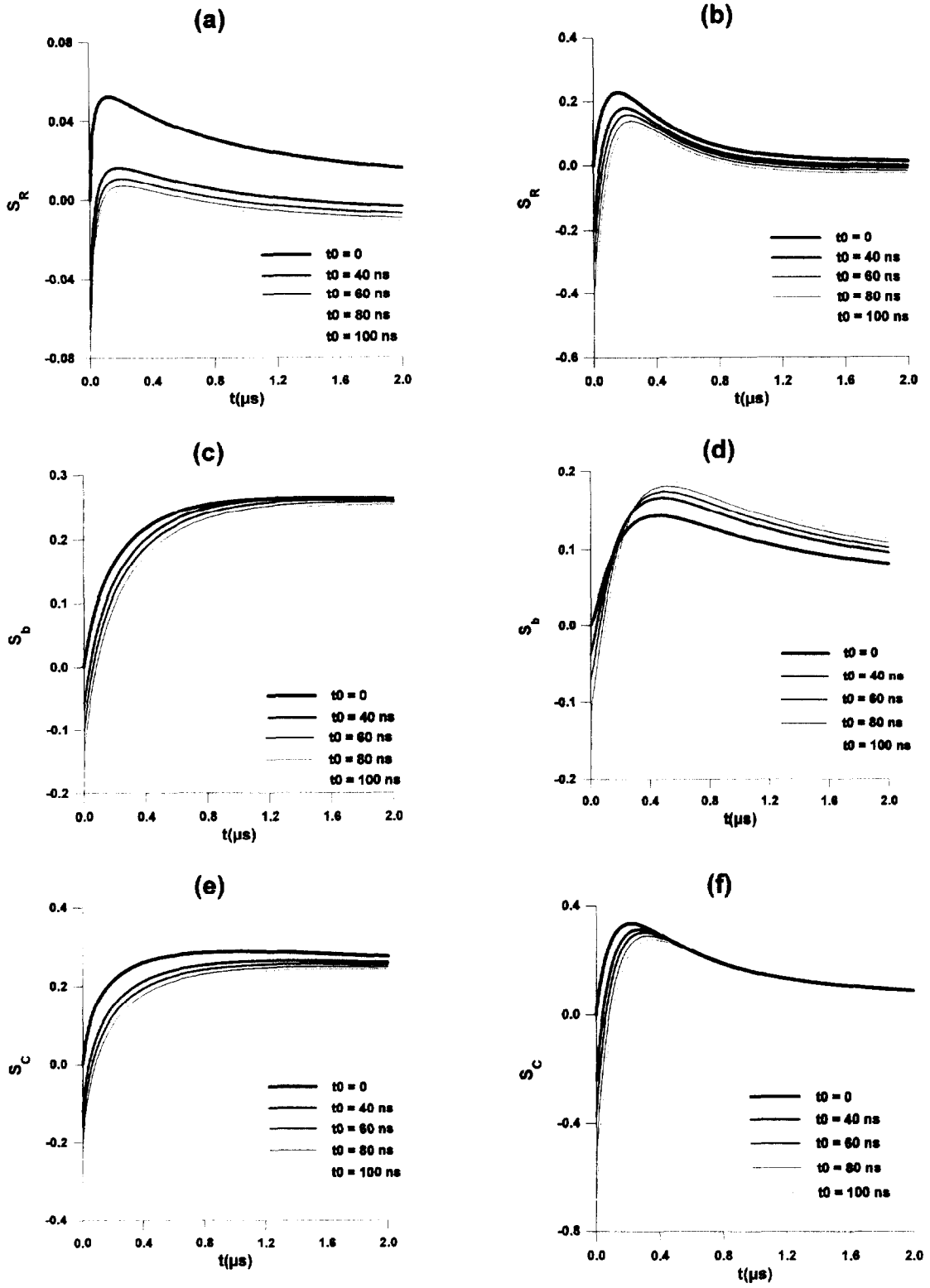

Fig. 14. Evolution of different sensitivity coefficients of reduced heatings $\theta(t)/\theta(t_0)$, (a) and (b) relative to the thermal interface resistance (S_R), (c) and (d) relative to the substrate effusivity (S_b), (e) and (f) relative to the coating thermal capacity (S_c), (a), (c), (e) 500 nm of copper on glass substrate, (b), (d), (f) 500 nm of copper on alumina substrate.

σ'_R is the random error and σ''_R the bias due to multi-dimensional effects. In assumption of a normal distribution of errors, σ'_R is given by:

$$\sigma'_R = \frac{R_c}{S_R}\sqrt{\left[\frac{\sigma_\theta^2}{\theta_0^2} + \frac{\sigma_{\theta_0}^2}{\theta_0^2}\left(\frac{\theta}{\theta_0}\right)^2 + \left(\frac{\sigma_t}{t}S_t\right)^2 + \left(\frac{\sigma_b}{b_2}S_b\right)^2 + \left(\frac{\sigma_c}{C_1}S_C\right)^2\right]} \quad (10)$$

which involves imprecision on the various parameters and the sensitivity coefficients. Imprecision on temperature measurement, depending on K value, is from 0.05–0.2°C (relation 3). Incertitude of θ_0 is about 0.2°C. Incertitude on the origin of the event is related to the sampling frequency fe. For fe = 50 MHz, σ_t is equal to 10 ns.

Relative incertitude on R_c, has a minimum which increases strongly in the low range of interface resistance (Fig. 15(a)). It seems that a ceramic substrate is more accurate. A copper film of 500 nm gives an incertitude of 20% on alumina and 50% on glass in the range of $R_c = 10^{-7}$ m^2 K W^{-1}. In addition, measurement of relative variations due to physical and chemical process is twice as accurate (Fig. 15(b)).

σ''_R mainly due to the one-directional assumption, may be approached by the relation:

$$\sigma''_R = \frac{R_c}{S_R}\left|\frac{\theta_1 - \theta'_1}{\theta_0}\right|. \quad (11)$$

The temperature difference $(\theta_1 - \theta'_1)/\theta_0$ does not exceed 1%. Small values of S_R, do that this systematic error is not always negligible. It can reach 10% but remains lower than the random error.

Threshold of detection is reached with $\alpha < 70$. The temperature rise is a few tens of degrees and its value is equivalent to noise and it is about 0.1°C. Thus, threshold is given by:

$$(R_c)_{\min} = \frac{c_1\rho_1 x_1}{70 c_2\rho_2\lambda_2}. \quad (12)$$

It is in the range of 10^{-7} m^2 K W^{-1} per μm of thin film on a polymer, $0.3 \cdot 10^{-7}$ m^2 K W^{-1} per μm on a glass and 10^{-9} m^2 K W^{-1} per μm on a ceramic. In practice, capability of recording do that it is in the range of 10^{-8} m^2 K W^{-1} per μm.

6. Experimental results

Glass and alumina (Al_2O_3 96%) substrates have been studied. Observations under electronic microscope show a smooth surface for glass and relieves for alumina surface due to granular structure (grain size from 200 nm to 1 μm) (Fig. 16). Roughness random mean square measurements have given $\sigma^* \approx 10$ nm for glass and $\sigma^* \approx 100$ nm for alumina. Microstructures of thin films are columnar (Fig. 17(a) and (b)), homogenous on glass and with porosity on alumina.

Incident pulse energy was about 400 mJ and provided temperature raising of 20–60 K. Absorptivity of thin films is strongly dependent on the microstructure. Alumina substrates lead to a higher absorption. A current supply from 50–100 mA has been used. It may be shown that Joule effect does not introduce any bias [13]. Methodology is a compromise between a good restitution of the signal and rejection of high frequency noises. Measurements have been achieved with 5–25 MHz analog bandwidth and 50 MHz sampling frequency. An attenuation and a delay of the peak occur under 5 MHz. Thermograms are disconcerted beyond 200 ns of the peak; so under 5 MHz identification is inaccurate. With 25 MHz, noises are superposed with the fundamental signal (Fig. 18) and thermogram may be analysed.

Parameter estimations need a relative thermogram θ/θ_0 which the reference θ_0 is taken from the early times after the peak. These thermograms are very sensitive to noises. It is the reason why, to reject high frequency noises, a signal processing of experimental data has been performed. A Gaussian filter has been used. Gauss method has been used for the parameter estimations during two microseconds of the cooling phase.

6.1. Non-contaminated structures

Clean structures (Fig. 19) give thermal interface resistances of about 10^{-7} m^2 K W^{-1} and effusivity corresponding to bulk materials (Table 1).

Uncertainties on R_c are evaluated to 45 and 30% for copper–glass and copper–alumina structures. Confidence intervals of effusivity are 5 and 10% for glass and alumina. Identification under various sequences leads to similar results (Table 2). Dispersion of 26 and 1% on R_c and b_2 (copper–glass structure) and of 4% and 1.2% (copper–alumina structure) has been observed.

Gauss method and a direct estimation of R_c have proved the validity of the model (Table 3) R_c appears as a constant parameter, conforming to the assumptions. In addition, data signal processing does not lead to some bias. Experimental and calculated relative temperatures (Fig. 19(a) and (c)) and residues of estimation (Fig. 19(b) and (d)) under a normalization θ_0 located at 100 ns from the origin show a good concordance in the sequence [0.1 μs; 2 μs]. Residues of the estimation are higher between 100 and 300 ns. This fact comes on the one hand from the sampling (50 MHz) and on the other hand from the filtering. Residues increase with alumina substrate because the experiment requires a faster sampling. A significant difference appears on R_c. $(R_c)_{\text{copper–glass}}$ is twice as high as $(R_c)_{\text{copper–alumina}}$. The roughness of alumina surface contributes to this fact because the metal penetrates into the inter-granular space and increases significantly

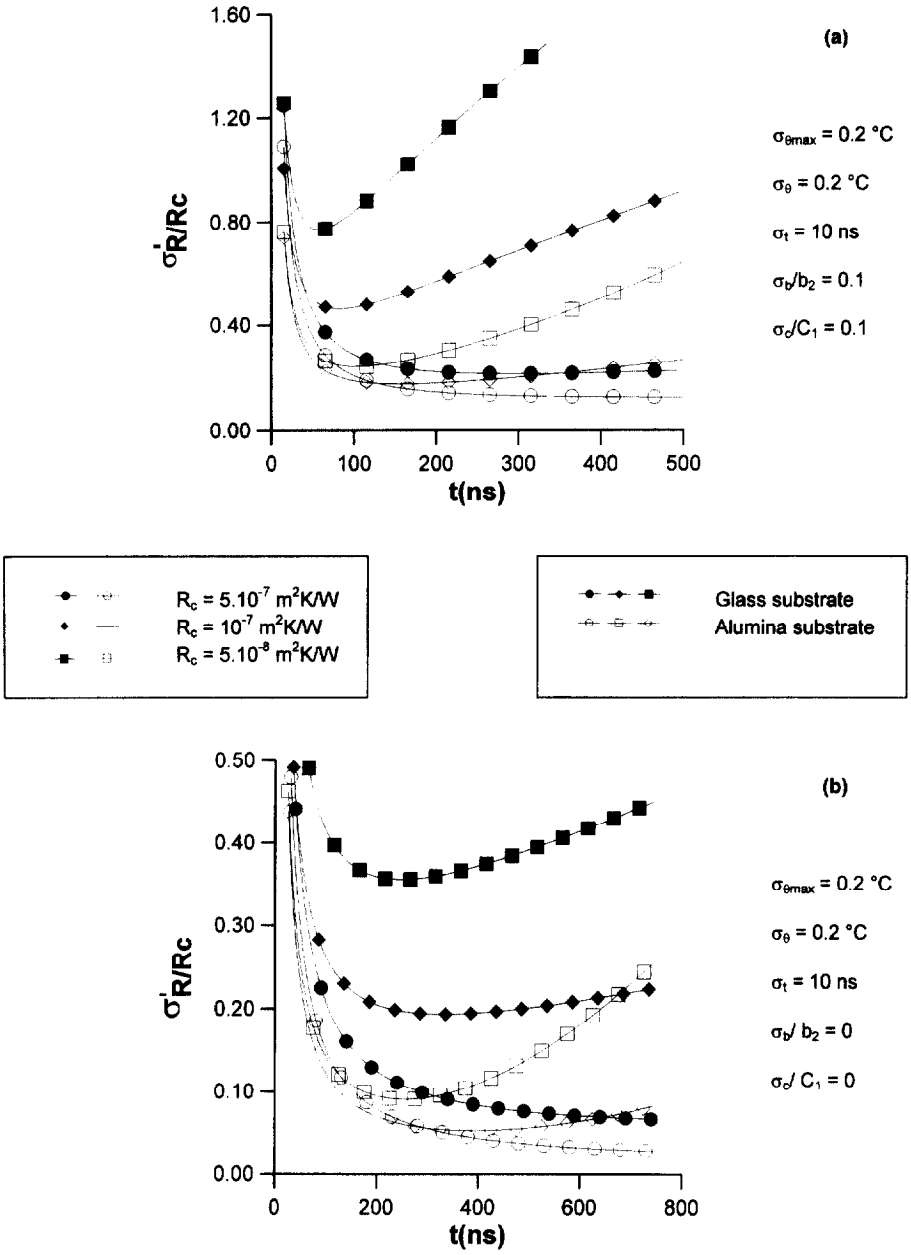

Fig. 15. Evolution of the relative uncertainties on the R_c measurement $x_1 = 500$ nm.

the contact surface. Moreover, microscopic observations do not let appear the non-adhesion regions.

6.2. Contamination effects

Effects of structural and chemical modifications (mechanical polish, contamination) have been studied.

6.2.1. Contamination of the substrate

Alumina has been polished by an Emery 120 paper. Microstructural modifications consist of the formation of a thin layer of ferrous oxide and the dislocation of grain joints in a few μm depth near the interface. These correspond to a decreasing of the apparent thermal conductivity. Significant differences appears on R_c and on effusivity (Table 4) because during experiments, heat

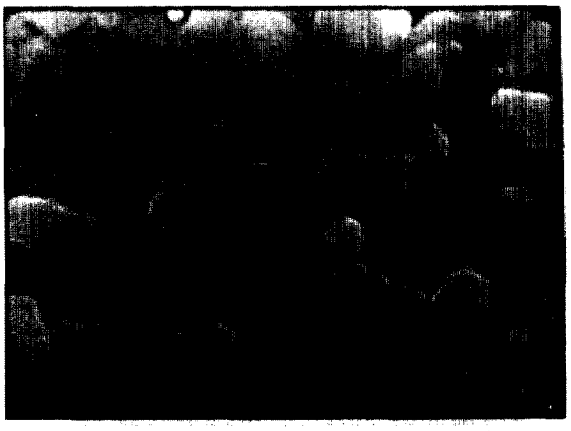

Fig. 16. Micrograph of the alumina surface (Al_2O_3 of 96%).

diffusion takes place inside a depth of 15 μm which corresponds to a few grain joints. Thus, measurements state a very sensitive effect on thermal properties of the structures.

6.2.2. Contamination of the thin film

Substrates have been contaminated by some organic molecules. The vacuum cell used under cathodic pulverization does not allow to extract all impurities. Impurities induce a deformation of the film and modify its thermophysical properties. Analysis show that the capacitive model remains valid [13]. The thermal capacity of the film has been extracted to obtain the same value of b. A lower thermal capacity and a higher interface resistance have been identified (Table 5). Measurements are similar in all sequences of identification. Relative

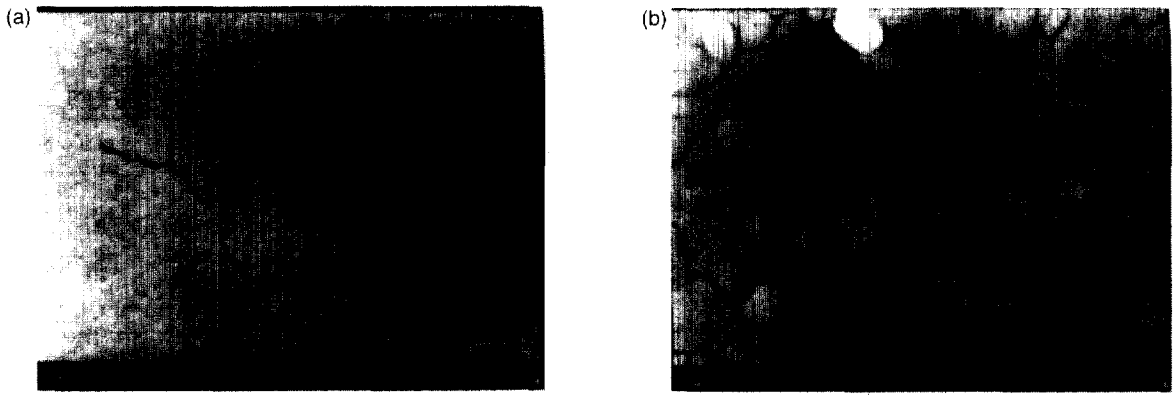

Fig. 17. Micrograph of the copper coating surface, (a) on a glass substrate, (b) on alumina substrate.

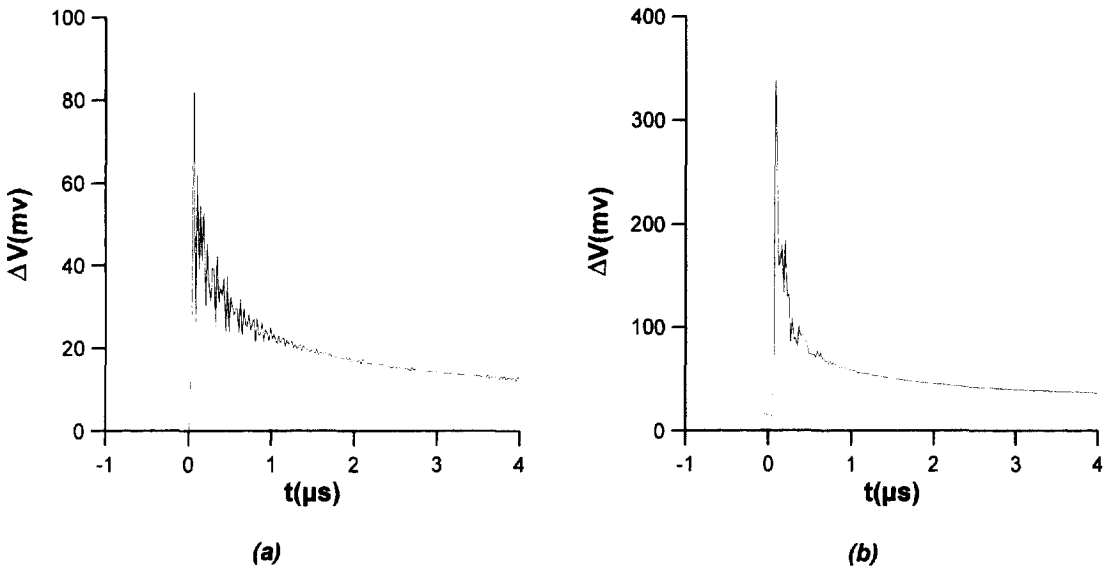

Fig. 18. Experimental thermograms (fc = 25 MHz). (a) Copper–glass, (b) copper–alumina, x_1 = 280 nm.

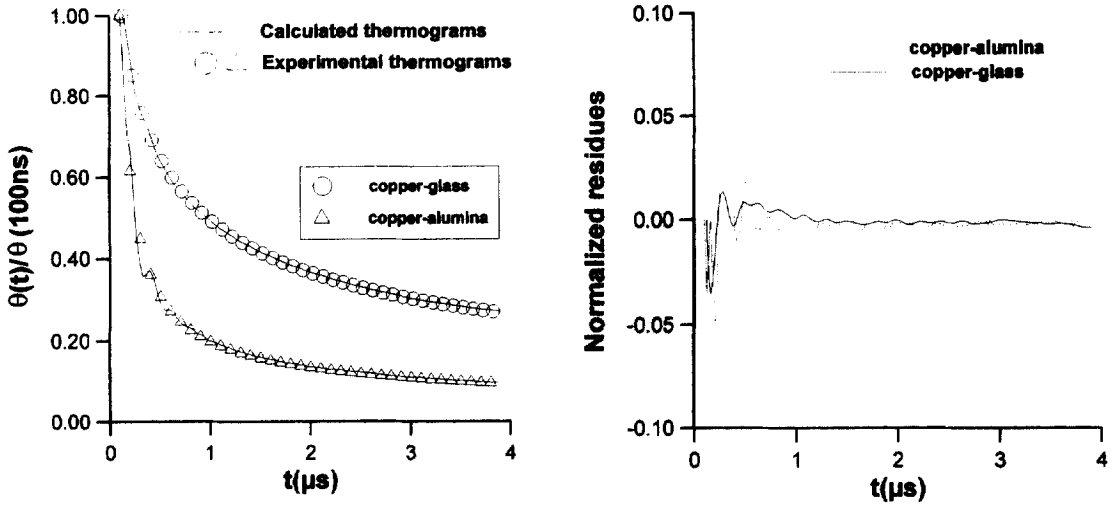

Fig. 19. Comparison of theoretical and experimental thermograms. Residues of the estimation.

Table 1
R_c and b_2 obtained with thermograms 18a and 18b. $c_1\rho_1 = 3.44 \cdot 10^{+6}$ (J m^{-3} K^{-1}), $x_1 \approx 280$ nm. Working time [0.1 μs; 2 μs]

Identified parameters	R_c (m^2 K W^{-1})	b_2 (J m^{-2} K^{-1} s$^{-1/2}$)	R_c (m^2 K W^{-1})	b_2 (J m^{-2} K^{-1} s$^{-1/2}$)
Structure	Copper–glass		Copper–alumina	
Tabulated values	—	1300–1600	—	7000–10 000
Identified values	$1.4 \cdot 10^{-7}$	1395	$6.14 \cdot 10^{-8}$	9382
Confidence intervals	$0.67 \cdot 10^{-7}$	77	$1.8 \cdot 10^{-8}$	933
Relative errors	47.8%	5.5%	29.3%	9.9%

Table 2
R_c obtained with thermograms 18a and 18b. $c_1\rho_1 = 3.44 \cdot 10^{+6}$ (J m^{-3} K^{-1}), $x_1 \approx 280$ nm. Different working time

Identified parameters	R_c (m^2 K W^{-1})	b_2 (J m^{-2} K^{-1} s$^{-1/2}$)	R_c (m^2 K W^{-1})	b_2 (J m^{-2} K^{-1} s$^{-1/2}$)
Structure	Copper–glass		Copper–alumina	
[100 ns; 1.2 μs]	$1.8 \cdot 10^{-7}$	1392	$6.36 \cdot 10^{-8}$	9296
[100 ns; 1.6 μs]	$1.52 \cdot 10^{-7}$	1392	$6.21 \cdot 10^{-8}$	9354
[100 ns; 2 μs]	$1.4 \cdot 10^{-7}$	1395	$6.14 \cdot 10^{-8}$	9382
[100 ns; 2.4 μs]	$1.31 \cdot 10^{-7}$	1399	$6.08 \cdot 10^{-8}$	9409
[100 ns; 2.8 μs]	$1.25 \cdot 10^{-7}$	1403	$6.03 \cdot 10^{-8}$	9430
[100 ns; 3.6 μs]	$1.2 \cdot 10^{-7}$	1408	$6.00 \cdot 10^{-8}$	9468

errors are about 20% for R_c and 7.5% for the thermal capacity.

7. Conclusions

An original method for experimental simultaneous determination of thermal interface resistance submicronic film-substrate and effusivity of the substrate has been set up. Effusivity is relative to depth of a few micrometers. The method is based on analysis of the transient temperature due to a laser pulse. Temperature measurement is deduced from the electrical resistance of the metallic film. In this way, thermal interface resistances as small as 10^{-8} m^2 K W^{-1} may be detected if analysis is performed before two microseconds. Detection uses a large analog bandwidth amplifier and a signal processing.

Table 3
Apparent thermal contact resistance obtained with b_2 and $c_1\rho_1 x_1$ fixed

Identified parameters	(a) Copper–glass structure			(b) Copper–alumina structure		
	$T(t)/T$ (100 ns)	$T(t)/T$ (200 ns)	$T(t)/T$ (300 ns)	$T(t)/T$ (100 ns)	$T(t)/T$ (200 ns)	$T(t)/T$ (300 ns)
$t = 1\ \mu s$	$1.08 \cdot 10^{-7}$	$1.11 \cdot 10^{-7}$	$1.01 \cdot 10^{-7}$	$6.22 \cdot 10^{-8}$	$6.77 \cdot 10^{-8}$	$7.00 \cdot 10^{-8}$
$t = 1.2\ \mu s$	$1.14 \cdot 10^{-7}$	$1.16 \cdot 10^{-7}$	$1.08 \cdot 10^{-7}$	$6.16 \cdot 10^{-8}$	$6.69 \cdot 10^{-8}$	$6.81 \cdot 10^{-8}$
$t = 1.4\ \mu s$	$1.04 \cdot 10^{-7}$	$1.06 \cdot 10^{-7}$	$9.81 \cdot 10^{-8}$	$6.00 \cdot 10^{-8}$	$6.49 \cdot 10^{-8}$	$6.38 \cdot 10^{-8}$
$t = 1.6\ \mu s$	$1.04 \cdot 10^{-7}$	$1.05 \cdot 10^{-7}$	$9.84 \cdot 10^{-8}$	$6.03 \cdot 10^{-8}$	$6.53 \cdot 10^{-8}$	$6.47 \cdot 10^{-8}$
$t = 1.8\ \mu s$	$1.05 \cdot 10^{-7}$	$1.07 \cdot 10^{-7}$	1.10^{-7}	$6.25 \cdot 10^{-8}$	$6.77 \cdot 10^{-8}$	$6.96 \cdot 10^{-8}$
$t = 2\ \mu s$	$8.41 \cdot 10^{-8}$	$8.48 \cdot 10^{-8}$	$7.58 \cdot 10^{-8}$	$6.10 \cdot 10^{-8}$	$6.60 \cdot 10^{-8}$	$6.62 \cdot 10^{-8}$

Table 4
R_c and b_2 of alumina. $c_1\rho_1 = 3.44 \cdot 10^{+6}$ (J m^{-3} K^{-1}), $x_1 \approx 280$ nm. Working time [0.1 μs; 2 μs]

Treatment of the surface	Non polished sample		Polished sample	
Identified parameters	R_c (m^2 K W^{-1})	b_2 (J m^{-2} K^{-1} s$^{-1/2}$)	R_c (m^2 K W^{-1})	b_2 (J m^{-2} K^{-1} s$^{-1/2}$)
Identified values	$6.14 \cdot 10^{-8}$	9382	$8.38 \cdot 10^{-8}$	6659

Table 5
R_c and $c_1\rho_1$. Working time [0.1 μs; 2 μs] $x \approx 280$ nm

Treatment of the surface	Non-contaminated structure			Contaminated structure		
Identified parameters	R_c	$c_1\rho_1$	b_2	R_c	$c_1\rho_1$	b_2
Identified values	$1.21 \cdot 10^{-7}$	$3.44 \cdot 10^{+6}$	1394	$7.91 \cdot 10^{-7}$	$2.5 \cdot 10^{+6}$	1396

The validity of the 1-D capacitive model has been proved and practical limitations have been evaluated.

Thermal interface resistances as small as 10^{-7} m^2 K W^{-1} on copper–glass and copper–alumina structures have been identified with an uncertainty of 30%. Effusivities of clean structures are conform with data of bulk materials. Effects of contamination have been observed and quantified. Variations of the interface resistance and effusivity, corresponding to chemical and structural modifications, have been detected. Relative measurements bring about the fore sensitive variations to the rate of impurities. In the future, experimental and theoretical studies will have to relate the thermophysical properties to chemical and physical structures.

Appendix

The complete model taken into account the 3-D effect into the substrate and given the spatial and temporal temperature profiles $T_1(x,t)$ and $T_2(x,y,z,t)$, in the thin film and its substrate, is the following:

(1)

$$\frac{\partial\theta_1(x,t)}{\partial t} - a_1\frac{\partial^2\theta_1(x,t)}{\partial^2 x} = \frac{Q(x,t)}{c_1\rho_1} \quad \forall -x_1 < x < 0, t > 0 \tag{A1.1.1}$$

$$\frac{\partial\theta_1}{\partial x} = 0 \quad \text{in } x = -x_1 \text{ plane} \tag{A1.1.2}$$

$$\frac{\theta_1(0,t) - \theta_2(0,y,z,t)}{R_c} = \varphi(y,z,t) \quad \text{in } x = 0 \tag{A1.1.3}$$

$$\text{at } t = 0 \quad \theta_1(x,0) = 0 \tag{A1.1.4}$$

(2)

$$\frac{1}{a_2}\frac{\partial\theta_2(x,y,z,t)}{\partial t} - \nabla^2\theta_2(x,y,z,t) = 0 \quad \forall x > 0, t > 0 \tag{A1.2.1}$$

$$-\lambda_2\frac{\partial\theta_2}{\partial x} = \varphi(y,z,t) \quad \text{on } A_1(x = 0, |y| \leqslant y_1, |z| \leqslant z_1)$$
$$= 0 \quad \text{everywhere} \tag{A1.2.2}$$

$$\frac{\partial\theta_2}{\partial y}=0 \quad \text{at } y=y_2 \quad \text{and} \quad y=-y_2 \tag{A1.2.3}$$

$$\frac{\partial\theta_2}{\partial z}=0 \quad \text{at } z=z_2 \quad \text{and} \quad z=-z_2 \tag{A1.2.4}$$

$$x\to\infty \quad \theta_2\to 0 \tag{A1.2.5}$$

$$\text{at } t=0 \quad \theta_2(x,0)=0 \quad \forall x>0. \tag{A1.2.6}$$

Q is the dissipation source per unit volume of the film. Its expression, for an optically thick medium, is given by:

$$Q(x,t)=\frac{(1-\rho_\lambda)P_0}{\pi r_0^2}\kappa_\lambda\{\exp[-(\kappa_\lambda x)]\}*f(t) \tag{A2}$$

in which κ_λ is the extinction coefficient, ρ_λ is the spectral reflectivity for the surface. $f(t)$ is temporal function. The temperature rise is:

$$\theta=T-T_i$$

T_i is an initial temperature. For convenience, T_i is taken uniform. Laplace transform is used:

$$\bar{\theta}_1(x,p)=\int_0^\infty \theta_1(x,\tau)e^{-p\tau}\,d\tau \tag{A3}$$

$$\bar{\theta}_2(x,y,z,p)=\int_0^\infty \theta_2(x,y,z,\tau)e^{-p\tau}\,d\tau. \tag{A4}$$

The solution of the transformed system (A2) is obtained by means of a double Fourier finite transformation realized in (y,z) plane:

$$\tilde{\bar{\theta}}_2(n,m)=\int_0^{y_2}\int_0^{z_2}\bar{\theta}_2\cos\frac{n\pi y'}{y_2}\cos\frac{m\pi z'}{z_2}\,dy\,dz. \tag{A5}$$

The transform of the solution of the system (A2) gives:

$$\begin{aligned}\bar{\theta}_2(x,y,z,p)=&\frac{\tilde{f}[\bar{\theta}_2(n=0,m=0)](x=0)}{y_2z_2}\\&+\frac{2}{y_2z_2}\sum_{n=1}^{\infty}\tilde{f}[\bar{\theta}_2(m=0)](x=0)\cos\frac{n\pi}{y_2}y\\&+\frac{2}{y_2z_2}\sum_{m=1}^{\infty}\tilde{f}[\bar{\theta}_2(n=0)](x=0)\cos\frac{m\pi}{z_2}\\&+\frac{4}{y_2z_2}\sum_{n=1}^{\infty}\sum_{m=1}^{\infty}\tilde{f}[\bar{\theta}_2(n,m)](x=0)\cos\frac{n\pi}{y_2}y\cos\frac{m\pi}{z_2}z.\end{aligned} \tag{A.6}$$

At the interface, uniformity of heat flux may be assumed. So, heat flux and temperature rise of the substrate are related by the following relation:

$$\bar{\theta}_2=\bar{F}\bar{\varphi} \tag{A7}$$

in which

$$\tilde{\bar{\theta}}_2(x=0)=\frac{1}{y_1z_1}\int_0^{y_1}\int_0^{z_1}\bar{\theta}_2(0,y',z')\,dy\,dz \tag{A8}$$

$\bar{F}$ is the transfer function film-substrate:

$$\begin{aligned}\bar{F}=&\frac{1}{\lambda_2\sqrt{\frac{p}{a_2}}}\frac{y_1z_1}{y_2z_2}+\frac{2}{\lambda_2\pi^2}\frac{y_2z_1}{y_1z_2}\sum_{n=1}^{\infty}\frac{\sin^2\frac{n\pi y_1}{y_2}}{n^2\sqrt{\left(\frac{n\pi}{y_2}\right)^2+\frac{p}{a_2}}}\\&+\frac{2}{\lambda_2\pi^2}\frac{y_1z_2}{y_2z_1}\sum_{m=1}^{\infty}\frac{\sin^2\frac{m\pi z_1}{z_2}}{m^2\sqrt{\left(\frac{m\pi}{z_2}\right)^2+\frac{p}{a_2}}}\\&+\frac{4}{\lambda_2\pi^4}\frac{y_2z_2}{y_1z_1}\sum_{n=1}^{\infty}\sum_{m=1}^{\infty}\frac{\sin^2\frac{n\pi y_1}{y_2}\sin^2\frac{m\pi z_1}{z_2}}{n^2m^2\sqrt{\left(\frac{n\pi}{y_2}\right)^2+\left(\frac{m\pi}{z_2}\right)^2+\frac{p}{a_2}}}.\end{aligned} \tag{A9}$$

Temperature calculations require a numerical inversion [15].

References

[1] Walker TW, Guenther AH, Nielsen PE. IEEE Journal of Quantum Electronics 1981;QE-17:2041.

[2] Lowdermilk WH, Milam D. IEEE Journal of Quantum Electronics 1981;QE-17:1888.

[3] Bardon JP. Proceedings of the Eurotherm Seminar No. 4 Thermal Transfer in Composite Materials at Solid Interface. Nancy: LEMTA, 1988, pp. 40–74.

[4] Bardon JP, Balageas D, Degiovanni A, Vullierme J. Colloque de Thermique des Systèmes et des Procédés 1988;285–99.

[5] Filk MI, Choi BI, Goodson, KE. Transactions of the ASME 1992;114(666).

[6] Phelan PE, Song Y, Nakabeppu O, Ito K, Hijikata K, Ohmori T, Torikoshi K. Transactions of the ASME 1994;116(1038).

[7] Swartz ET, Pohl RO. Appl. Phys. Lett. 1987;51(26).

[8] Swartz ET, Pohl RO. Reviews of Modern Physics 1989;61(3).

[9] Leung WP, Tam AC. Optics Letters 1984;9(3).

[10] Leung WP, Tam AC. Journal of Applied Physics 1988;63(9):4505–10.

[11] Tam AC, Sontag H. Applied Physics Lett 1986;49(26):1761–3.

[12] Boley and Weiner. NY: Wiley 1967, 4éme edition.

[13] Hmina N. Ph.D. thesis, December, 1994.

[14] Hmina N, Scudeller Y. J Phy III 1995;5:881–901.

[15] Stehfest H. Gaver. Commun A.C.M. 13, 1970;47:49.

[16] Scudeller Y, Hmina N. Heat Transfer, 3rd U.K. National Conference Incorporating 1st European Conference on Thermal Sciences 1992;2:1189–95.

[17] Hmina N, Scudeller Y. 1ére Conférence Maghrébine de génie des Procédés 1994;1:327–30.

[18] Qiu TQ, Tien CL. International Journal of Heat and Mass Transfer 1992;35:719–26.